Electronic Supplementary Material (ESI) for Nanoscale.

Supporting Information

for

Superior Li-ion storage of VS_4 nanowire anchored on reduced graphene

Guang Yang [a†], Huanhuan Wang [a,c†], Bowei Zhang [a], Shini Foo [a], Mingbo Ma [a], Xun Cao [a], Jilei Liu [b*], Shibing Ni[,d], Srinivasan Madhavi [a,e*], Yizhong Huang [a*]

[a] School of Materials Science and Engineering, Nanyang Technological University, 50 Nanyang Avenue, Singapore 639798

[b] College of Materials Science and Engineering, Hunan province key laboratory for advanced carbon materials and applied technology, Hunan University, Changsha, 410082, China

[c] CINTRA CNRS/NTU/Thales, UMI 3288, 50 Nanyang Drive, 637553, Singapore

[d] College of Materials and Chemical Engineering, China Three Gorges University, Yichang, 443002, China

[e] Energy Research Institute @ NTU (ERI@N), Nanyang Technological University, Research Techno Plaza, 50 Nanyang Drive, Singapore 637553

† These authors contributed equally.

* Corresponding authors: liujilei@hnu.edu.cn (J. Liu), Madhavi@ntu.edu.sg (S. Madhavi), and YZHuang@ntu.edu.sg (Y. Huang)

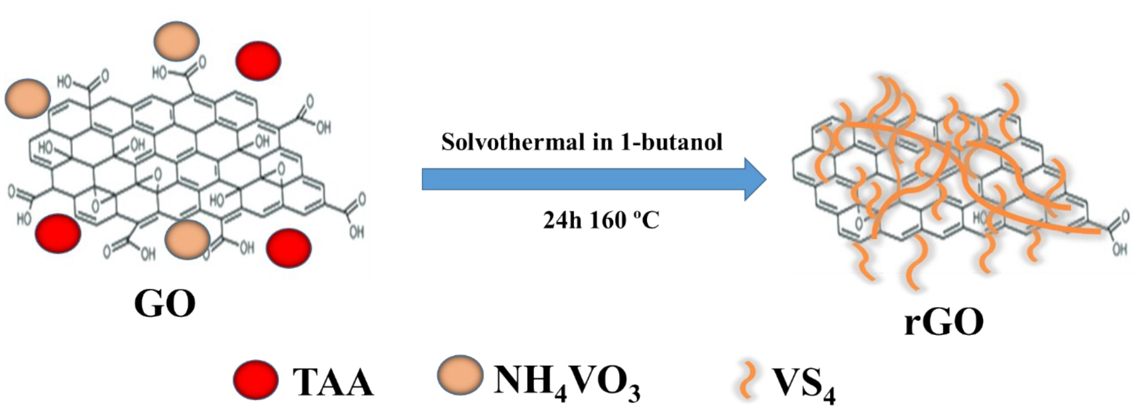

Fig. S1 Schematic illustration for the fabrication of VS_4 anchored on reduced graphene.

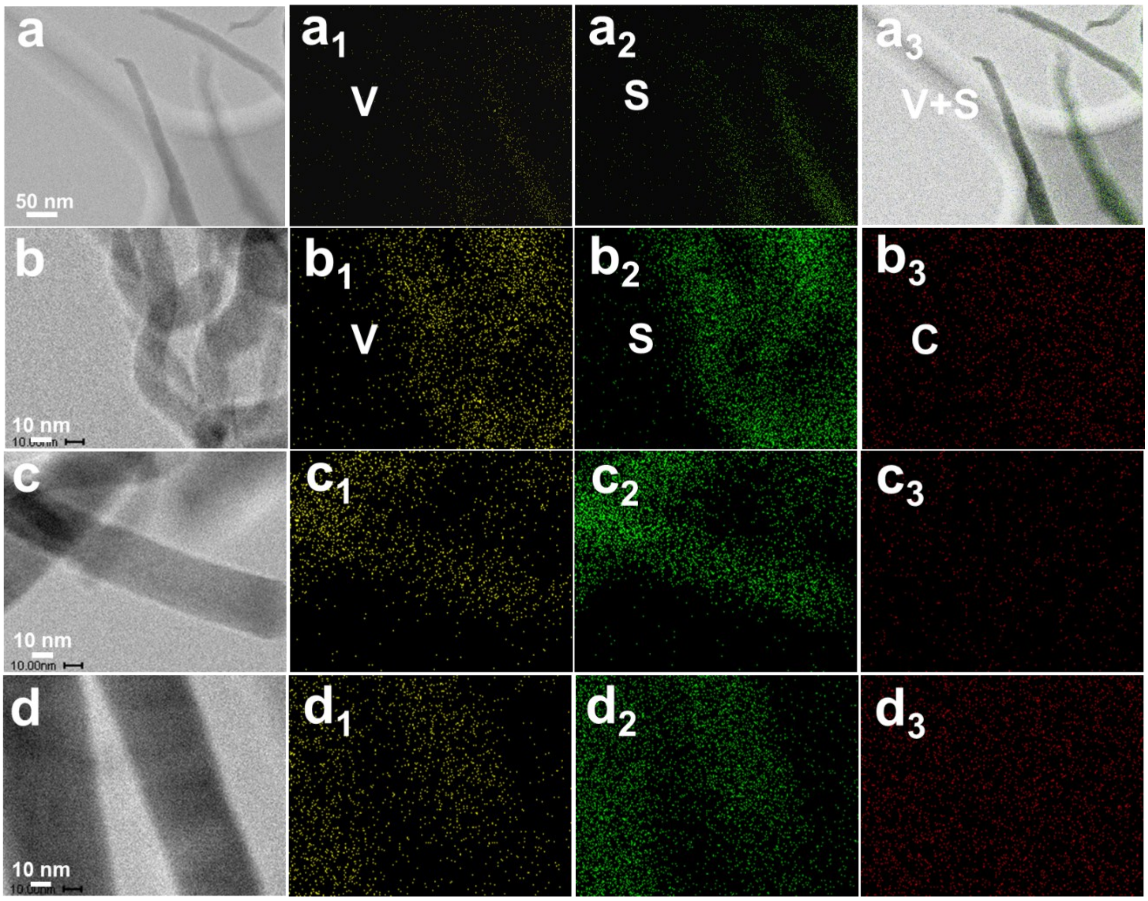

Fig. S2 SEM images and the corresponding EDS elemental mapping of (a, a1, a2, a3) V, S and V+S for VS_4; and V, S, and C for (b, b1, b2, and b3) VS_4@5rGO; (c, c1, c2, and c3) VS_4@15rGO, and (d, d1, d2, and d3) VS_4@35rGO.

Table S1 FTIR peaks and their assignments.

Peaks	Band assignment	Reference
1631	δ(OH)	1
1400	Amorphous carbon	1
1200	C-O-R	2
980	S^{2-}(V-S-V)	2-4
550	Terminal S stretching	2-4

ν: stretching; δ: bending.

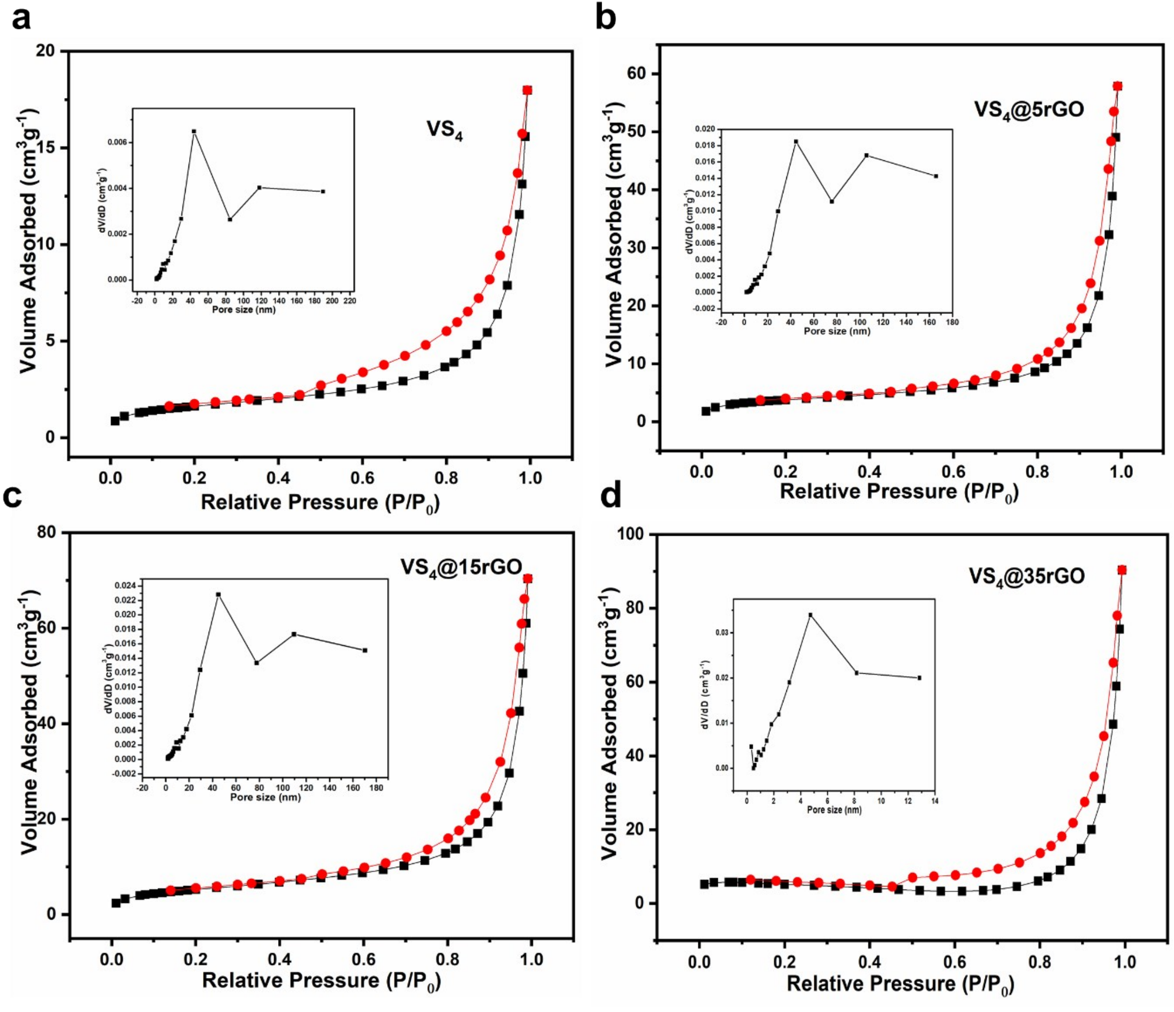

Fig. S3 The Nitrogen-adsorption-desorption isotherms of the (a) VS$_4$, (b) VS$_4$@5rGO, (c) VS$_4$@15rGO, and (d) VS$_4$@35rGO. The insets are their corresponding pore size distribution.

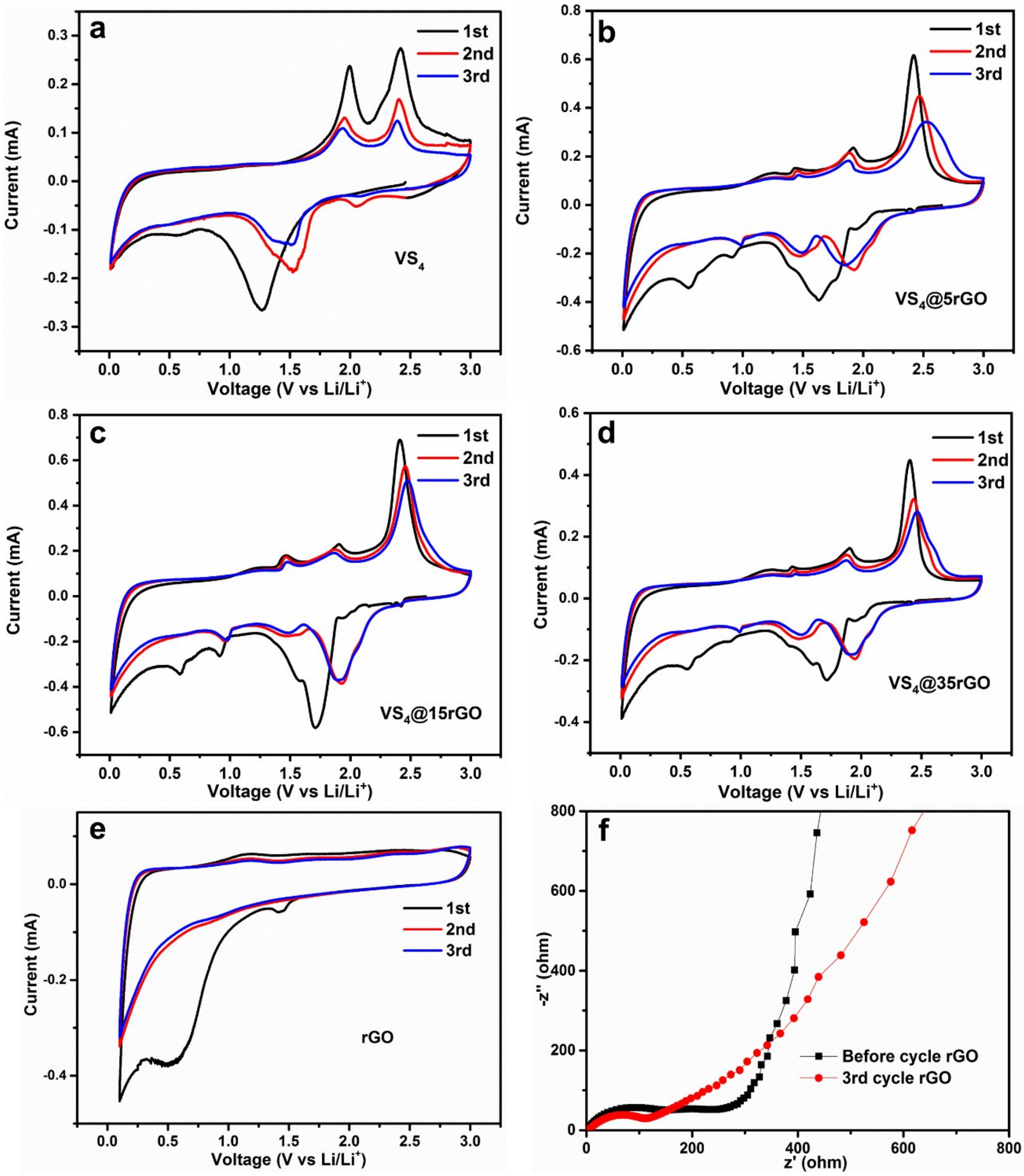

Fig. S4 First three CVs of (a) VS$_4$, (b) VS$_4$@5rGO, (c) VS$_4$@15rGO, and (d) VS$_4$@35rGO and (e) rGO as well as the (f) EIS before cycle and after 3 cycles of CV scanning with a scan rate of 0.2 mV s^{-1} in the voltage range of 0.01-3.00 V vs Li/Li$^+$.

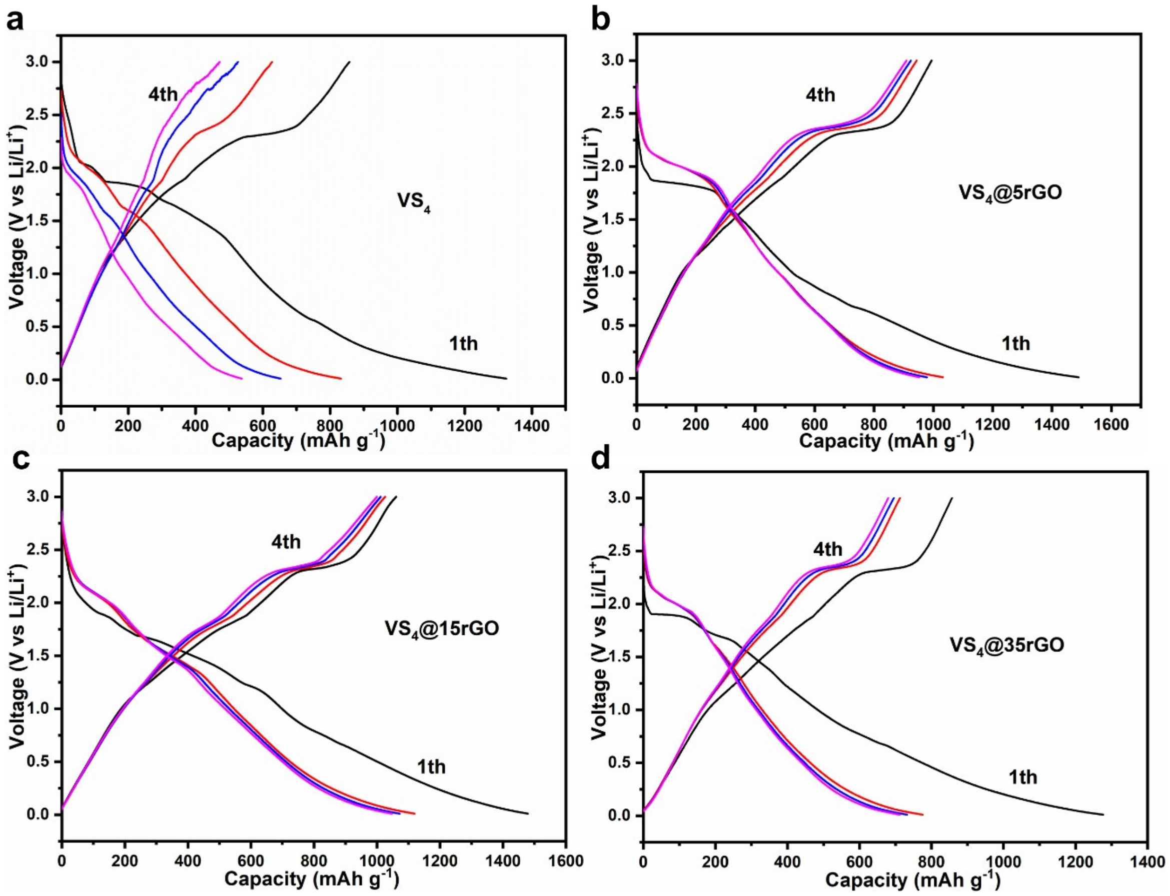

Fig. S5 First four galvanostatic discharge-charge profiles at a current rate of 0.1 A g^{-1} in the voltage range of 0.01-3 V vs Li/Li^+ for: (a) VS_4; (b) VS_4@5rGO; (c) VS_4@15rGO; (d) VS_4@35rGO.

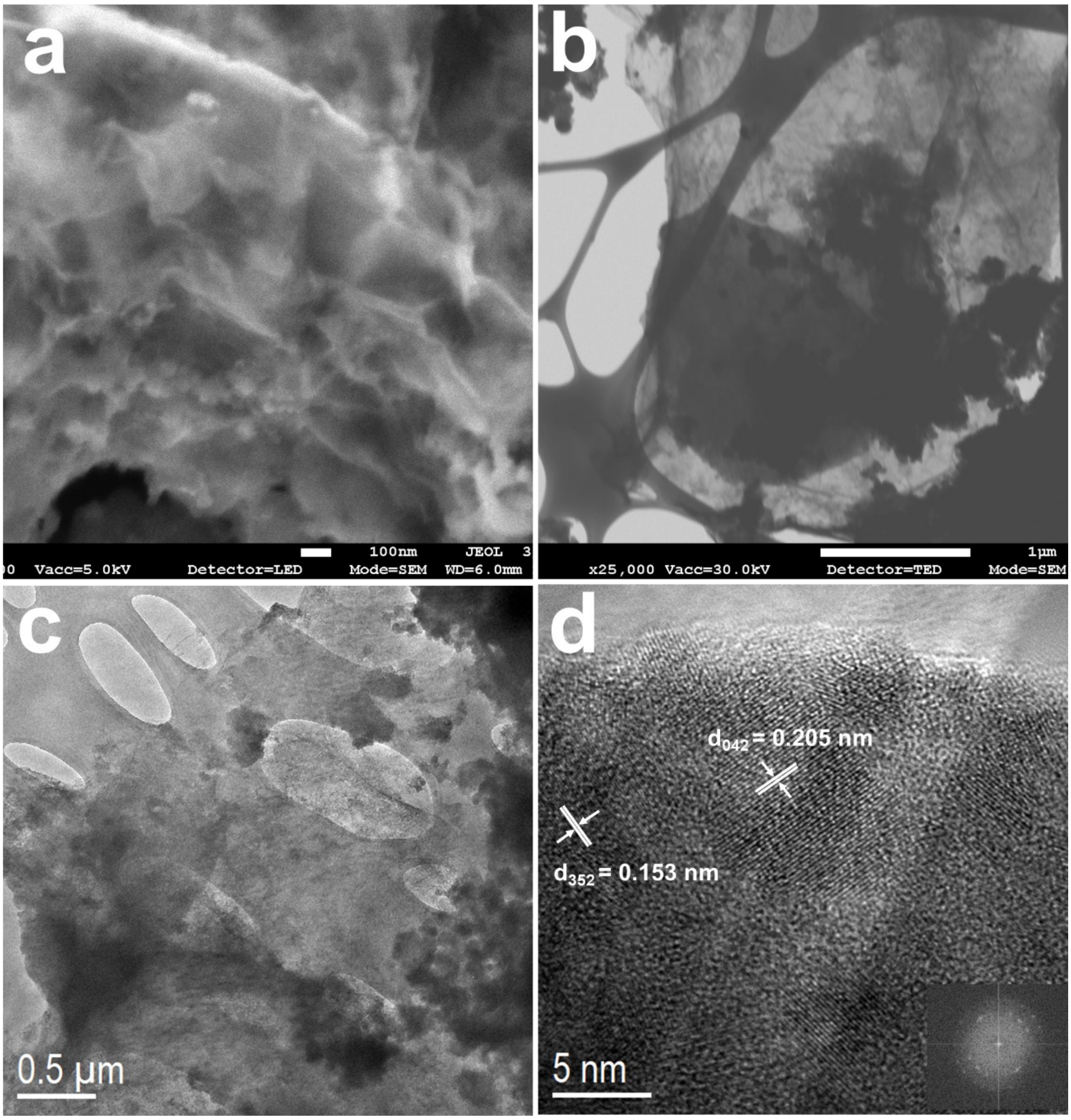

Fig. S6 VS$_4$@15rGO after 100 cycles at a current of 0.1 A g-1 (a3) SEM image in LED mode; (b3) SEM image in TED mode; (c3) TEM image; (d3) HRTEM image showing the d-spacing of 0.153 nm and 0.205 nm in the (352) and (042) plane, respectively (inset: FFT image).

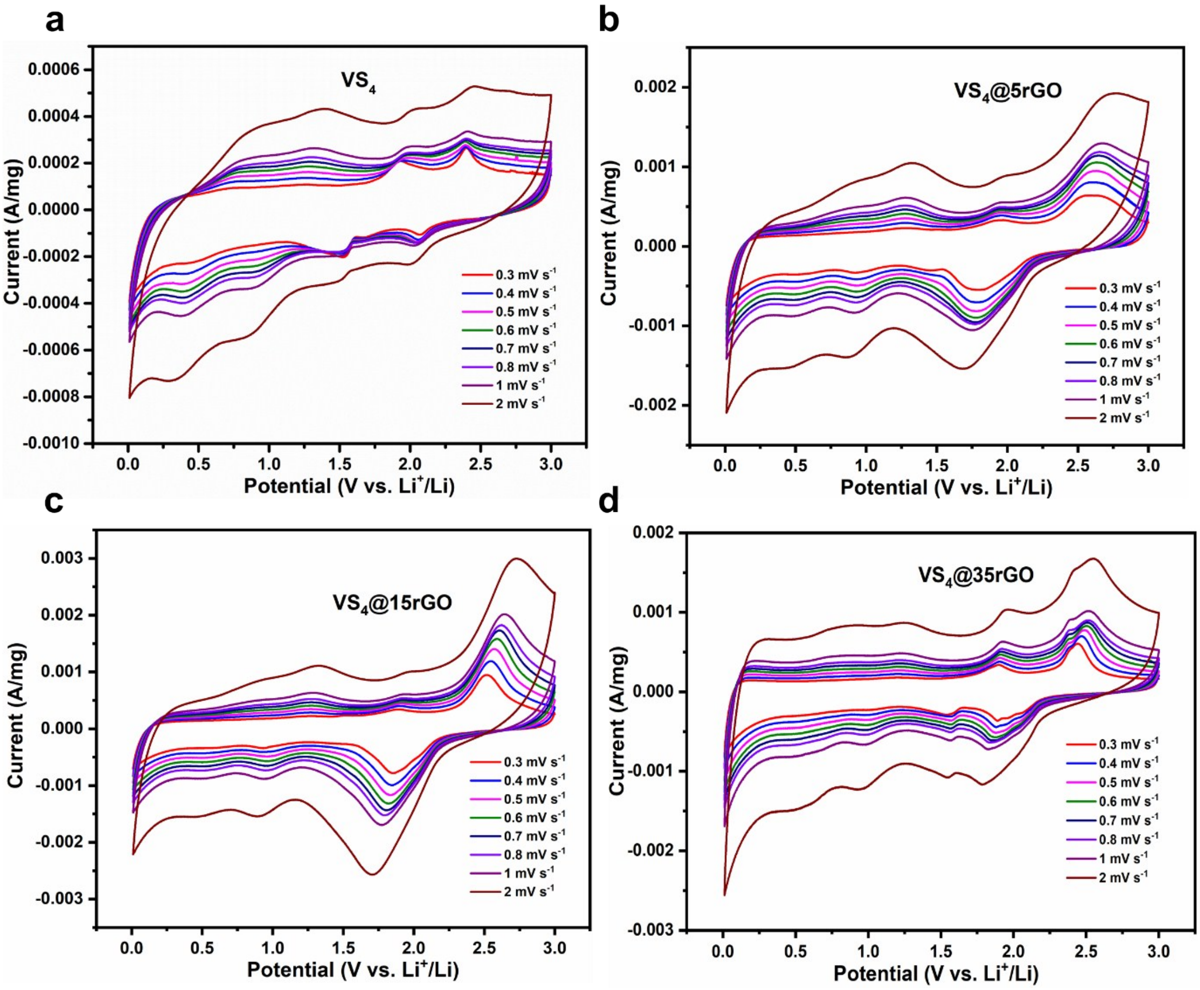

Fig. S7 CV curves of (a) VS_4; (b) VS_4@5rGO; (c) VS_4@15rGO; (d) VS_4@35rGO at different scan rates between 0.01 to 3.00 V;

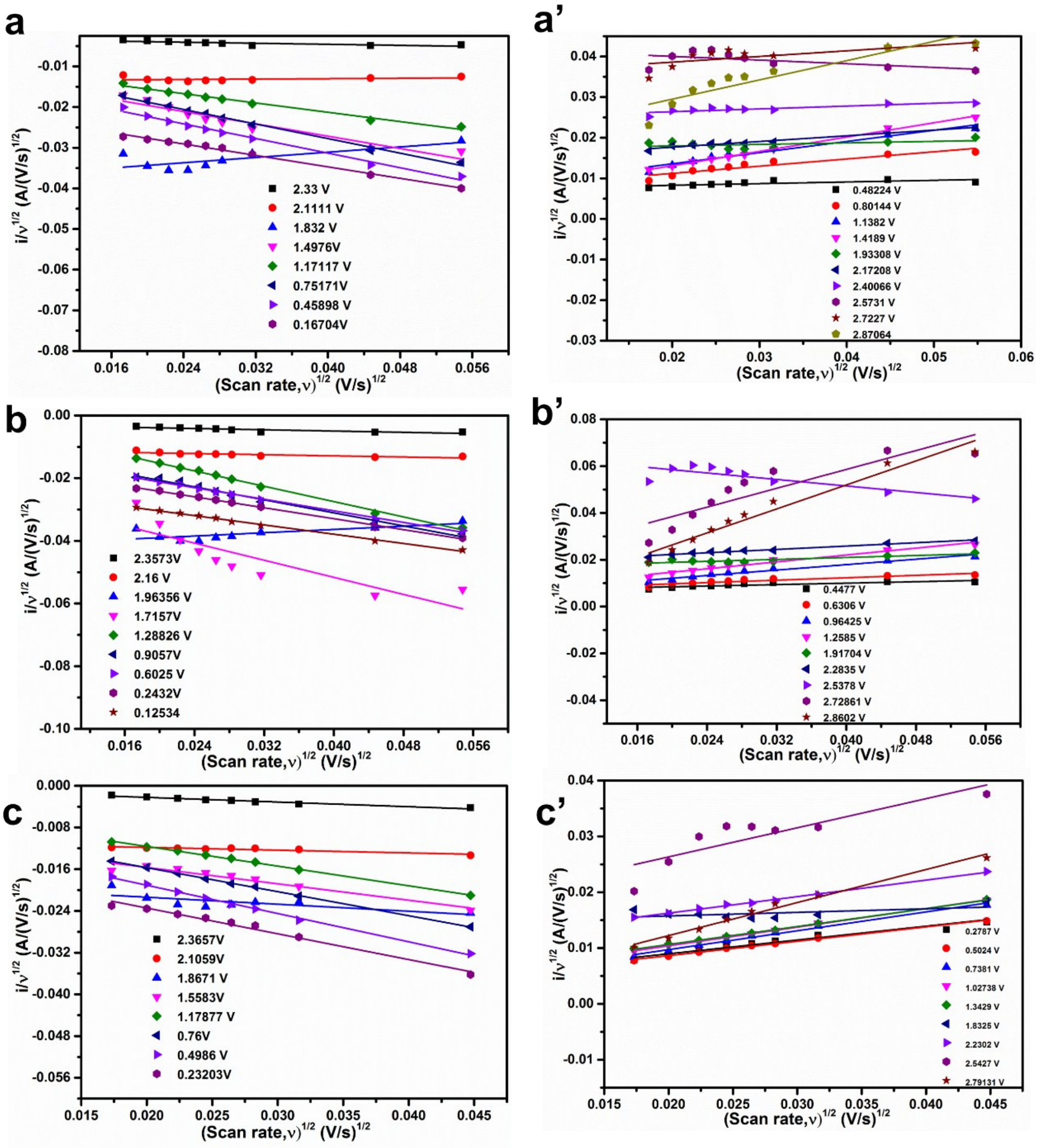

Fig. S8 (a, a’), (b, b’), and (c, c’) are the plots of $\nu^{1/2}$ vs $i/\nu^{1/2}$ for VS$_4$@5rGO, VS$_4$@15rGO, and VS$_4$@35rGO at both anodic and cathodic scan. The plots are used for calculating constants k_1 and k_2 at different potentials of the cathodic scan and anodic scan.

The total current at a fixed potential can be described using the following equation: $I(V) = k_1\nu + k_2\nu^{1/2}$, where $k_1\nu$ and $k_2\nu^{1/2}$ represent the capacitive contribution and intercalation contribution, respectively. The k_1 and k_2 can be obtained from the slope and y-axis intercept of the straight line: $i(V)/\nu^{1/2} = k_1\nu^{1/2} + k_2$, as shown in Fig. S6. Thus, the contribution from capacitive and intercalation can be calculated, and each component contribution at a scan rate of 0.3 mV/s is shown in Fig. 3f.

XPS survey scanning (Fig. S9) and fine scanning for C, V and S elements (Fig. S10) were conducted for pristine VS_4@15rGO, after discharged at 0.01 V and charged to 3 V. From the survey scan (Fig. S9), it is observed that the main peaks correspond to sulfur, vanadium, carbon, and oxygen in VS_4@15rGO.[5] After being discharged to 0.01 V, fluorine peaks are apparent and oxygen peaks become stronger. This is reasonable because SEI forms during discharging, where some $LiPF_6$ electrolyte decompose when contact with electrode materials and form fluoride and oxide based by product.[6, 7] Also, the vanadium peaks become very weak after discharging, this could be due to the formation of nanocrystal vanadium metal after discharging, which are embedded within the particle and too small difficult to detect. Even 5 mins Ar ion bombarding, the vanadium peaks are still weak. When VS_4@15rGO is further charged to 3 V. the vanadium peak looks more obvious.

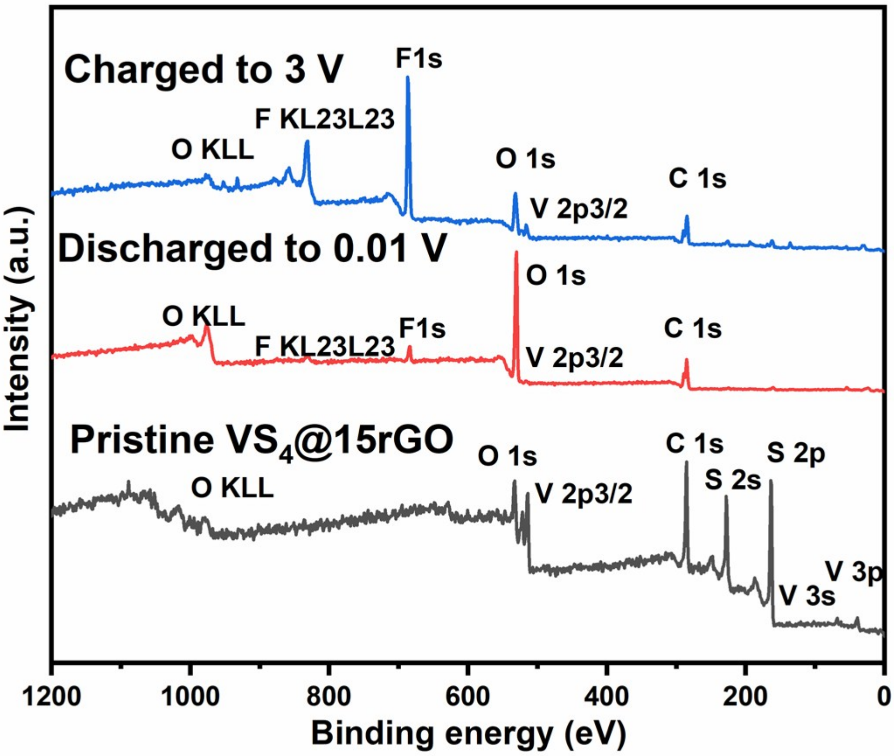

Fig. S9 XPS survey spectrum of VS_4@15rGO at pristine, after discharged at 0.01 V and charged to 3 V.

To analyze the process of redox reaction, the C 1s, scanning of V 2p and S 2p spectrum of VS_4@15rGO at pristine, after being discharged to 0.01 V and charged to 3 V (Fig. S10) are carried out by XPS. For the pristine VS_4@15rGO, the C 1s core level spectrum can be deconvoluted into three components at 284.8 eV, 287.1 eV and 289.0 eV (Fig. S10a), corresponding to the C–C, C–O and O–C=O groups, respectively.[8, 9] It should be noted that the intensity of C–C is higher compared to that of C–O and O–C=O in pristine sample because of C-C bond in rGO. Comparing with the samples at 0.01 V and 3 V (Fig. S10b and c), the intensities of C–O and O–C=O of pristine is lower, which is because no super p amorphous carbon is added in pristine VS_4@15rGO and rGO has lower content of C–O and O–C=O than super p amorphous carbon. Three oxidation states of vanadium species are seen after peak separation of the V 2p core level spectrum, as depicted in Fig. S10a1. The two peaks centered at 517.3 eV and 524.3 eV are correlated with the 2p3/2 and 2p1/2 components of V^{4+}. Also, the vanadium 2p1/2 peaks located at 522.9 eV with relatively low intensity can be attributed to V^{3+} species, arising from the partial reduction of the vanadium source to V^{3+} in solvothermal reaction.[10] Meanwhile, the two strong peaks at 514 eV and 521.5 eV are ascribed to the 2p3/2 and 2p1/2 components of the V–C bond, similar to previous study.[10] Noticeably, the intensity of the V–C component is even higher than that of V^{4+}, which could be associated with the strong bonding between VS_4 and rGO substrate. With the sample being discharged to 0.01 V, vanadium could be reduced to metal. However, instead of vanadium metal, only V^{3+} is detected by XPS. This could be resulted from the oxidization of vanadium metal nanocrystal with trace of oxygen (Fig. S10b1). After the electrode being charged back to 3 V, V^{4+} is detected, which means some VS_4 is reformed (Fig. S10c1). For the sulfur element in pristine VS_4@15rGO (Fig. S10a2), S 2p core level analysis shows two peaks at 162.9 eV and 164.1 eV, in good agreement with sulfur 2p3/2 and 2p1/2 of the S_2^{2-} dimer in VS_4. When being discharged to 0.01 V (Fig. S10b2), the peaks of 159.8 and 161.7 eV appear and are attributed to the S 2p doublet in Li_2S. S_2^{2-} are reformed after charged to 3 V (Fig. S10c2).[11]

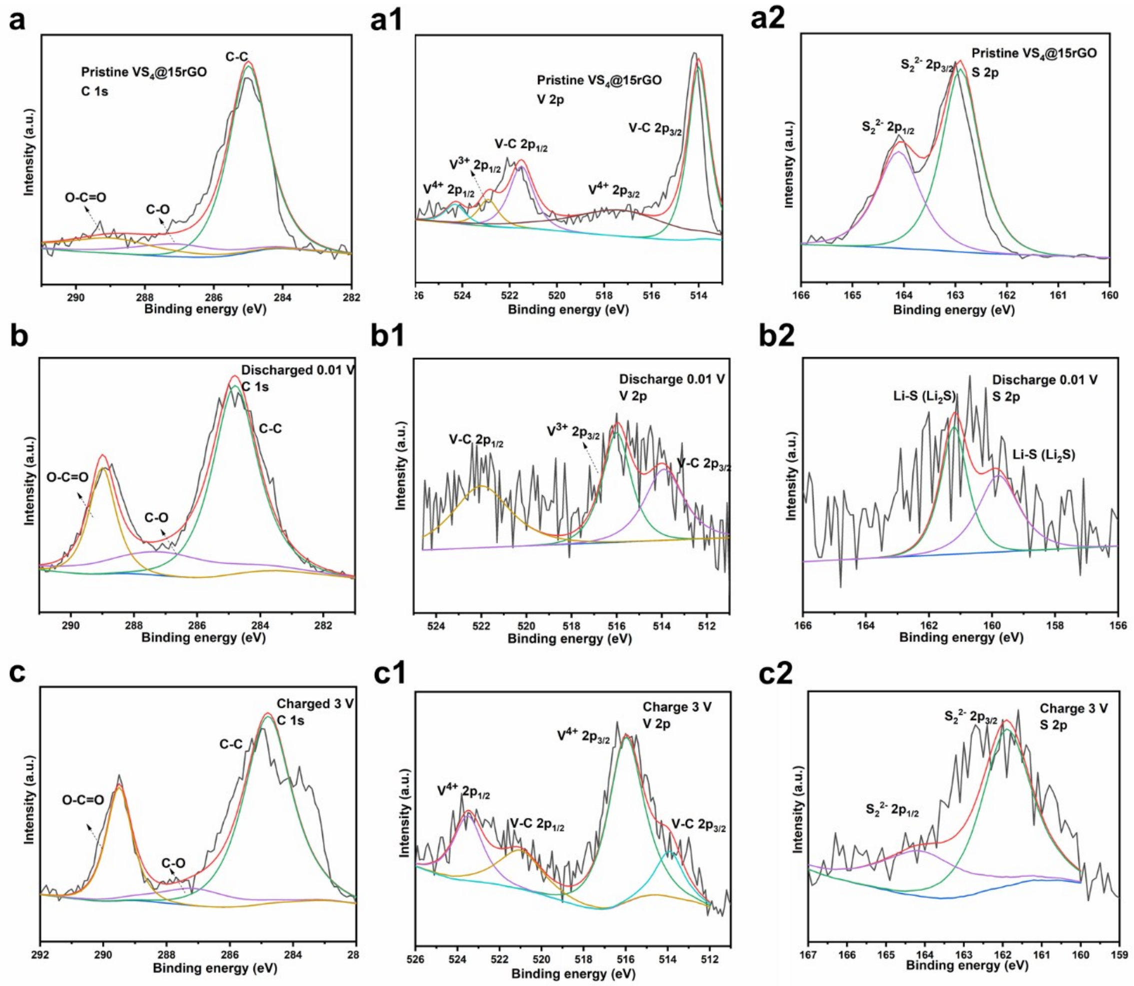

Fig. S10 The C 1s, V 2p and S 2p spectrum of VS$_4$@15rGO (a, a1, a2) at pristine, after discharged at (b, b1, b2) 0.01 V and charged to (c, c1, c2) 3 V.

References

1. Q. Li, Q. Wei, J. Sheng, M. Yan, L. Zhou, W. Luo, R. Sun and L. Mai, *Adv. Sci.*, 2015, **2**, 1500284.

2. Y. Zhou, Y. Li, J. Yang, J. Tian, H. Xu, J. Yang and W. Fan, *ACS Appl. Mater. Interfaces*, 2016, **8**, 18797-18805.

3. W. Fang, H. Zhao, Y. Xie, J. Fang, J. Xu and Z. Chen, *ACS Appl. Mater. Interfaces*, 2015, **7**, 13044-13052.

4. G. Lui, G. Jiang, A. Duan, J. Broughton, J. Zhang, M. W. Fowler and A. Yu, *Industrial & Engineering Chemistry Research*, 2015, **54**, 2682-2689.

5. H. Qin, Z. Yang, L. Chen, X. Chen and L. Wang, *J. Mater. Chem. A*, 2018, **6**, 23757-23765.

6. E. Peled and S. Menkin, *J. Electrochem. Soc.*, 2017, **164**, A1703-A1719.

7. M. Nie, D. P. Abraham, Y. Chen, A. Bose and B. L. Lucht, *J. Phys. Chem. C*, 2013, **117**, 13403-13412.

8. K. Zhu, H. Qiu, Y. Zhang, D. Zhang, G. Chen and Y. Wei, *ChemSusChem*, 2015, **8**, 1017-1025.

9. S. Pei and H.-M. Cheng, *Carbon*, 2012, **50**, 3210-3228.

10. Q. Pang, Y. Zhao, Y. Yu, X. Bian, X. Wang, Y. Wei, Y. Gao and G. Chen, *ChemSusChem*, 2018, **11**, 735-742.

11. K. Han, J. Shen, C. M. Hayner, H. Ye, M. C. Kung and H. H. Kung, *J. Power Sources*, 2014, **251**, 331-337.